

University of South Florida

From the Selected Works of Yonggang Liu

2005

Momentum balance diagnoses for the West Florida Shelf

Yonggang Liu, *University of South Florida*

Robert H Weisberg, *University of South Florida*



Available at: <https://works.bepress.com/yliu/9/>

Momentum balance diagnoses for the West Florida Shelf

Yonggang Liu*, Robert H. Weisberg

College of Marine Science, University of South Florida, St. Petersburg, FL 33701, USA

Received 24 June 2004; received in revised form 2 December 2004; accepted 4 March 2005

Abstract

The momentum balance over the West Florida Shelf is diagnosed using observations of currents, bottom pressures, temperatures, winds, and coastal sea levels, along with hydrographic data from 32 monthly cruises spanning summer 1998 to winter 2001. Over synoptic weather time scales, the depth-averaged across-shelf momentum balance on the inner shelf is essentially geostrophic with smaller contributions from the across-shelf wind stress and other terms. Coherence analyses show that 95% of the acceleration (Coriolis and local) variance may be accounted for by the pressure gradient and friction (surface and bottom) over the synoptic weather band. The balances are more complicated on the outer shelf where the Coriolis, across-shelf bottom pressure gradient and horizontal density gradient terms all have the same magnitude. Over synoptic and longer time scales, the depth-averaged along-shelf momentum balance on the inner shelf is mainly between the wind stress and bottom friction with smaller contributions from the pressure gradient, local acceleration and Coriolis terms. The along-shelf pressure gradient is mainly set up by the local along-shelf wind stress. These balances enable us to estimate the depth-averaged, along-shelf currents on the inner shelf from the winds and coastal sea level or from the winds and across-shelf bottom pressure gradient, or from both. The across-shelf sea level gradient may also be inferred from the wind and coastal sea level data.

© 2005 Elsevier Ltd. All rights reserved.

Keywords: Momentum balance; Observations; Circulation dynamics; Coastal oceanography; West Florida Shelf

1. Introduction

Continental shelf momentum balance analyses have been diagnosed from observations for the South Atlantic Bight (Lee et al., 1984, 1989), the Pacific Northwest (Hickey, 1984), the Celtic Sea (Thompson and Pugh, 1986), and the coastal oceans of northern California (Lentz, 1994; Trowbridge and Lentz, 1998; Lentz and Trowbridge, 2001), North Carolina (Lentz et al., 1999), and New Jersey

(Tilburg and Garvine, 2003). It is widely accepted that the depth-averaged, across-shelf momentum balance at outer and mid-shelf locations is predominantly geostrophic, with the Coriolis force due to the along-shelf currents balancing the across-shelf pressure gradient force (Thompson and Pugh, 1986; Brown et al., 1985, 1987; Lee et al., 1984, 1989; Lentz et al., 1999). In the along-shelf direction the momentum balance tends to be frictional. On the Northern Carolina inner shelf the wind stress and pressure gradient are balanced by bottom stress, with flow accelerations becoming increasingly important offshore (Lentz et al., 1999). This is in contrast with the central Southern California Bight,

*Corresponding author. Tel.: +1 727 553 1627;
fax: +1 727 553 1189.

E-mail address: yliu18@gmail.com (Y. Liu).

where variations in along-shelf pressure gradient account for a larger fraction of the along-shelf velocity variations than the local wind stress (Hickey et al., 2003).

All continental shelves have their own nuances due to their geometries and boundary currents. The West Florida Shelf (WFS) is broad and gently sloping with the Gulf of Mexico Loop Current at times impinging on the shelf slope (Molinari et al., 1977; Huh et al., 1981; Paluszkiwicz et al., 1983; Hetland et al., 1999; He and Weisberg, 2003; Weisberg and He, 2003), and with the fresh water of the Mississippi River influencing the mid-shelf in spring and summer (Gilbes et al., 1996; He and Weisberg, 2002a). Previous observational inferences on WFS momentum balances are limited. For instance, Mitchum and Sturges (1982) analyzed three weeks of current meter data from two moorings at the 22 and 44 m isobaths and concluded that the dominant momentum balance in the along-shelf direction is between the wind and bottom stresses.

Li and Weisberg (1999a,b) reported on WFS momentum analyses using a three-dimensional primitive equation model forced by idealized upwelling (and downwelling) favorable winds. When forced by a steady and spatially uniform southeastward along-shelf wind stress, the vertically integrated across-shelf momentum balance is primarily geostrophic independent of water depth. The along-shelf momentum balance is essentially Ekman (a balance between the wind stress and the Coriolis acceleration terms) over the mid to outer shelf, whereas the balance is between the wind and bottom stresses near shore. The inner shelf is found to be the region within which the surface and bottom Ekman layers interact. Offshore of Sarasota, Florida the inner shelf extends out to about the 50 m isobath. When forced by a steady and spatially uniform offshore wind stress, the vertically integrated across-shelf momentum balance is depth dependent. The mid to outer shelf shows an Ekman balance, while on the inner shelf, the Coriolis term decreases as the pressure gradient term increases, and in the near shore the balance is between the wind stress and the pressure gradient terms with the Coriolis term playing a secondary role. In the along-shelf direction, the bottom stress term becomes of increasing importance with decreasing depth over the inner shelf; on the mid-shelf the balance is primarily Ekman, and further offshore on the shelf slope the local acceleration is relatively large and spatially

variable due to vortex stretching. Additional model momentum balances under stratified conditions are reported by Weisberg et al. (2000, 2001). However, these model results are not yet verified by observations.

The acquisition of long time series now facilitate diagnostic calculations of WFS momentum balances with in situ data. Hourly time series of velocity, bottom pressures, bottom temperatures, and winds, along with hydrographic data from 32 monthly cruises allow us to consider the momentum balances at several locations across the shelf. These analyses provide further insight into the nature of the WFS dynamics. An overview of the observations and a description of data processing are given in Section 2. The relevant equations are derived in Section 3. Across- and along-shelf momentum balances are analyzed in Sections 4 and 5, respectively, and applications are made in Section 6. Bottom friction parameters are estimated in Section 7. Section 8 then discusses the results and Section 9 provides a summary.

2. In situ observations and data processing

Concurrent programs on the WFS aimed at studying harmful algae blooms and other property variations provided velocity and other data from up to 13 moorings beginning in summer 1998. Fig. 1 shows the mooring locations and Table 1 provides supporting information. There are data from five bottom-mounted moorings (EC5, EC6, EC4, NA1 and NA3) on the inner shelf, each with an upward looking acoustic Doppler current profiler (ADCP) measuring currents over most of the water column at 0.5 m intervals, along with temperature, salinity, and pressure near the bottom. On the outer shelf, there are two subsurface moorings (CM4 and EC1) with upward looking ADCPs located 4 m from the bottom, measuring currents in 5 m intervals over most of water column, along with temperature, salinity, and pressure at the ADCP depth. From the 25 to 50 m isobaths, there are surface buoys (NA2, EC3, EC2, CM2 and CM3) with downward-looking ADCPs measuring currents throughout most of the water column, along with winds at the surface.

Wind observations are from two NOAA/NDBC stations 42036 and VENF1 (Venice) (<http://www.ndbc.noaa.gov/>) and from the USF surface buoys. Hydrographic data are from monthly cruises from June 1998 through December 2001 in which conductivity–temperature–depth (CTD) profiles

Table 1
Mooring information

Mooring name	Water depth (m)	Latitude (N)	Longitude (W)	Good bins (m)	Pr. sensor depth (m)	Overall observation period
EC6	10	26°24.5'	82°12.5'	3–8	9.5	09/15/1998–08/23/2001
EC5	10	27°17.9'	82°38.4'	3–8	9.5	07/14/1998–03/17/2002
EC4	20	27°11.2'	82°47.8'	3–18	19.5	07/13/1998–03/19/2002
NA1	25	27°12.0'	82°56.7'	3–23	24.5	07/13/1998–08/25/2001
NA2	25	27°09.8'	82°55.5'	3–23	—	09/14/1998–12/05/2001
NA3	25	27°07.7'	82°54.0'	3–23	24.5	07/13/1998–08/25/2001
EC3	30	27°01.8'	82°59.8'	3–27	—	09/14/1998–12/06/2001
EC2	50	26°56.9'	83°23.0'	5–45	—	05/12/1999–12/06/2001
CM4	78	26°45.1'	83°49.4'	10–60	74.6	06/25/2000–09/11/2001
EC1	162	26°33.5'	84°14.9'	15–145	157.8	06/25/2000–06/25/2001

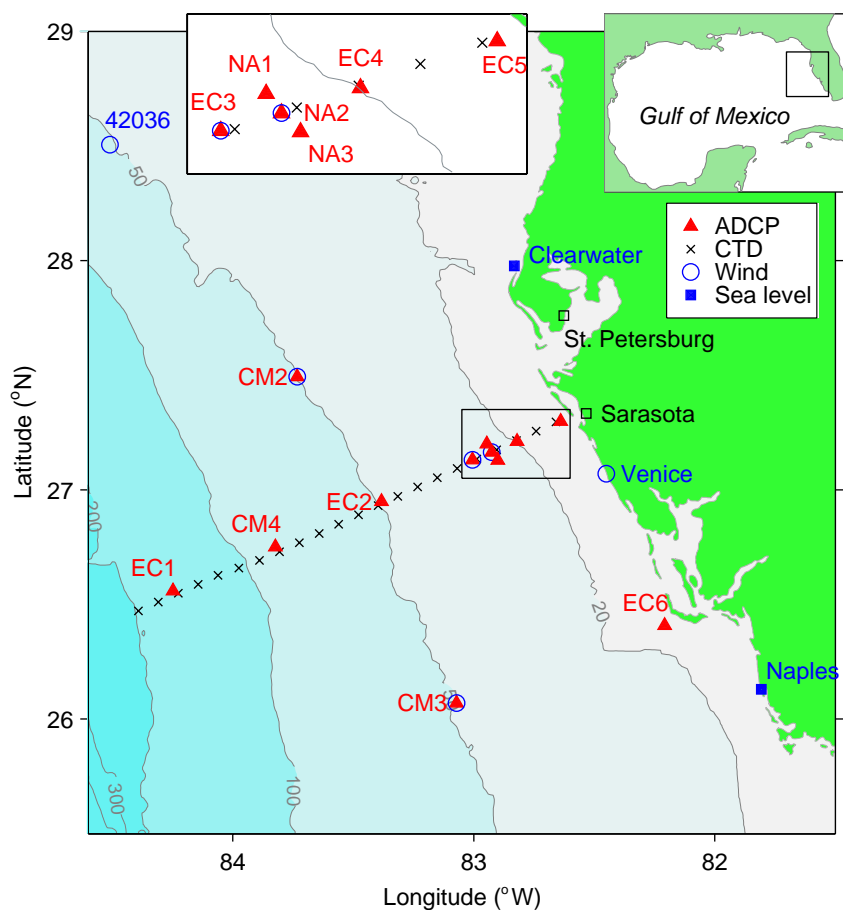


Fig. 1. Map of the WFS showing bottom topography, ADCP mooring stations, CTD transect offshore Sarasota, wind and coastal sea level stations. Enlarged inner WFS near Sarasota is shown as an inset map in the upper-left corner. The relative location of the WFS is shown in a Gulf of Mexico map inserted in the upper-right corner.

were generally taken along three across-shelf transects, and the station locations relevant to the ADCP moorings are also shown in Fig. 1. Coastal sea level data at Clearwater and Naples are from the NOAA/NOS (<http://www.co-ops.nos.noaa.gov/>).

Editing of the ADCP velocity data consisted of bin mapping to standard depths (by interpolation) and eliminating (side-slope) contaminated data either near the surface (for the bottom-mounted) or near the bottom (for the surface-buoys). Principal

axes of variance were calculated from depth-averaged, 36-h low-pass filtered data, and the angles made by the semi-major axes are used to define the along-shelf directions at each of the mooring sites. These generally aligned with the isobaths.

Editing of the bottom pressure data began with inspection to remove the records deemed incorrect due to contamination from sand inundation or battery failures toward the end of deployments. An atmospheric pressure correction was then made using nearby air pressure records. These records were then de-meaned and de-tided by removing the four major tide constituents: M2, S2, K1 and O1, using the Tide Harmonic Analysis Toolbox of Pawlowicz et al. (2002). We then had to contend with trends in some of the deployments. Methods dealing with pressure sensor drift are found in Wearn and Larson (1982) and Harms and Winant (1994). However, fully objective methods for correcting bottom pressure records do not exist (Brown et al., 1987). In our case, with several deployments ranging from 2 to 14 months duration, we opted for a method of piecewise detrending to eliminate unknown long time interval variations without destroying the synoptic weather band. Instead of detrending an entire deployment, the time series were divided into two or more subsets, and each subset was detrended individually. The length of a subset depended on the data quality. The longest subset was 6 months, while the shortest subset was less than 1 month. After applying piecewise detrending and 36-h low-pass filtering, all the bottom pressure records were joined together to form a single long time series for each mooring location.

Each of the bottom pressure sensors also recorded bottom temperature and conductivity. All of the bottom temperature records agreed with the shipboard CTD observations at similar depths. Biofouling and in some cases sand contamination degraded the moored salinity data during the later part of each deployment. Rather than attempt to edit these effects we inferred the bottom density from the temperature data. For each mooring location, a linear $T-\sigma_t$ relationship was obtained by a least-squares fit of the near bottom temperature with σ_t from the nearest CTD observation over all of the hydrographic cruises. These $T-\sigma_t$ relationships were then applied to the bottom temperature time series to derive time series of bottom density for each mooring.

Two wind stress time series were formed for the inner and outer shelves, respectively. For the inner

shelf, the NA2 buoy winds were primarily used; when NA2 winds were not available, wind data from buoy EC3 was used instead; when neither NA2 nor EC3 winds were available, an average wind from the other five available records was used. Similarly, for the outer WFS, an average wind between stations CM2 and CM3 was used, and when neither of these winds was available, an average wind from the other four available records was used instead.

For all of the hourly time series, small gaps of up to a few hours were filled by linear interpolation. For consistency in the across-shelf momentum balances all the hourly time series were piecewise detrended (as with the bottom pressure), de-meaned, and 36-h low-pass filtered. Current velocity time series were further rotated for across- and along-shelf components according to the current principal axes at individual sites. Wind vectors were converted to an oceanographic direction convention (the direction to which wind is blowing) and then rotated 27° clockwise for across- and along-shelf components. Given these data preparations the across-shelf momentum analyses apply to the time scales of the synoptic weather band. In contrast to the across-shelf momentum balances, since coastal sea level is used instead of the bottom pressure for most of the along-shelf momentum balance calculations, the piecewise detrending is not applied, such that the along-shelf momentum balances also apply to the time scales longer than the synoptic weather band.

3. Momentum balance equations

Via the hydrostatic assumption, the pressure at depth z can be computed from bottom pressure p_b , water column depth h , and internal density structure (Brown et al., 1985)

$$p(z) = p_b - \rho_0 g(z + h) - g \int_{-h}^z \rho' dz, \quad (1)$$

where g is the gravitational acceleration, ρ_0 is a reference density, and $\rho'(x, y, z, t)$ is a small density anomaly due to spatial and temporal variability, such that $\rho = \rho_0 + \rho'(x, y, z, t)$. Here x and y denote the across- and along-shelf directions, respectively, with x positive onshore and y positive northward, z denotes the vertical direction, positive upward and zero at the surface. By differentiating Eq. (1) along x , and vertically integrating over the

water column, the across-shelf pressure gradient is

$$\begin{aligned} \left\langle \frac{\partial p}{\partial x} \right\rangle &= \frac{1}{H} \int_{-h}^{\eta} \frac{\partial p}{\partial x} dz \\ &= \frac{\partial p_b}{\partial x} - \rho_0 g \frac{\partial h}{\partial x} - \frac{g}{H} \int_{-h}^{\eta} \left[\frac{\partial}{\partial x} \int_{-h}^z \rho' dz' \right] dz, \end{aligned} \quad (2)$$

where $H = \eta + h$ is the total water depth. The depth-averaged momentum equations, excluding the nonlinear acceleration terms, are

$$\frac{\partial \bar{u}}{\partial t} - f \bar{v} = -\frac{1}{\rho_0} \left\langle \frac{\partial p}{\partial x} \right\rangle + \frac{\tau_s^x}{\rho_0 H} - \frac{\tau_b^x}{\rho_0 H}, \quad (3a)$$

$$\frac{\partial \bar{v}}{\partial t} + f \bar{u} = -\frac{1}{\rho_0} \left\langle \frac{\partial p}{\partial y} \right\rangle + \frac{\tau_s^y}{\rho_0 H} - \frac{\tau_b^y}{\rho_0 H}, \quad (3b)$$

where (τ_s^x, τ_s^y) , and (τ_b^x, τ_b^y) are the surface and bottom stresses, $\langle \partial p / \partial x \rangle$ and $\langle \partial p / \partial y \rangle$ are the depth-averaged pressure gradients, (\bar{u}, \bar{v}) are depth-averaged velocities, and f is the Coriolis parameter. Substituting Eq. (2) into Eq. (3a), and removing temporal mean values, leads to the perturbation equation

$$\begin{aligned} \frac{\partial \bar{u}}{\partial t} - f \bar{v} &= -\frac{1}{\rho_0} \frac{\partial p_b}{\partial x} + \frac{g}{\rho_0 H} \int_{-h}^{\eta} \frac{\partial}{\partial x} \left[\int_{-h}^z \rho' dz' \right] dz \\ &\quad + \frac{\tau_s^x}{\rho_0 H} - \frac{\tau_b^x}{\rho_0 H}, \end{aligned} \quad (4)$$

where all the variables in Eq. (4) are now understood to be deviations from the temporal mean state. Applying Leibniz's rule to the baroclinic term gives

$$\begin{aligned} \frac{\partial \bar{u}}{\partial t} - f \bar{v} &= -\frac{1}{\rho_0} \frac{\partial p_b}{\partial x} + \frac{g}{\rho_0 H} \int_{-h}^{\eta} \int_{-h}^z \frac{\partial \rho'}{\partial x} dz' dz \\ (a) \quad (b) \quad (c) \quad (d) \\ &\quad + \frac{g \rho'_h}{\rho_0} \frac{\partial h}{\partial x} + \frac{\tau_s^x}{\rho_0 H} - \frac{\tau_b^x}{\rho_0 H}, \\ (e) \quad (f) \quad (g) \end{aligned} \quad (5)$$

where $\rho'_h = \rho'(-h)$ is bottom density anomaly. On the left-hand side (LHS), terms (a) and (b) are the local acceleration and Coriolis terms, respectively. On the right-hand side (RHS), terms (c)–(g) are bottom pressure gradient, horizontal density gradient, bottom buoyancy, wind stress, and bottom stress terms, respectively. The sum of the first three terms on the RHS (c)+(d)+(e), is the pressure gradient term.

The bottom buoyancy term arises from the deviation of the seabed from a level reference surface ($\partial h / \partial x \neq 0$) and can vary through time with

ρ'_h (Thompson and Pugh, 1986). With the bottom slope $\partial h / \partial x$ between moorings EC4 and EC5 being about 0.5×10^{-3} (10 m/20 km), a ρ'_h of magnitude 1 kg m^{-3} , results in a bottom buoyancy term of $5 \times 10^{-6} \text{ m s}^{-2}$, which, for the latitude of WFS, is equivalent in magnitude to the Coriolis term under a velocity of 7 cm s^{-1} . Thus, changes of ρ'_h are potentially important and should be monitored if the pressure sensors are sited on a sloping bottom. A similar term, with a different definition of ρ'_h , is derived and its significance in calculating bottom velocity transport on continental shelves is addressed by Mellor et al. (1982) and Morison (1991). All of the terms in Eq. (5) are now relatable to the observed variables: velocity [terms (a), (b) and (g)], bottom pressure [term (c)], CTD data [term (d)], bottom temperature (density) data [term (e)], and winds [term (f)].

For the along-shelf direction, upon removing the temporal mean values from Eq. (3b), the resulting perturbation equation remains the same form. Near the coast, the along-shelf pressure gradient may be assumed to be constant throughout the water column, and approximated by the along-shelf sea level gradient, $\langle \partial p / \partial y \rangle = \rho_0 g \partial \eta / \partial y$, where η is sea level.

4. Across-shelf momentum balance

4.1. Estimation of terms

Since we must differentiate pressure time series between moorings, we define (for consistency) a new velocity time series between adjacent moorings by averaging velocity time series from the two sites, (\bar{u}_1, \bar{v}_1) , and (\bar{u}_2, \bar{v}_2) , weighted by the water depths, h_1 and h_2 , i.e.,

$$(\bar{u}, \bar{v}) = \left(\frac{\bar{u}_1 h_1 + \bar{u}_2 h_2}{h_1 + h_2}, \frac{\bar{v}_1 h_1 + \bar{v}_2 h_2}{h_1 + h_2} \right).$$

The local acceleration term $\partial \bar{u} / \partial t$ is computed through forward difference in the time domain. The bottom pressure gradient term can be estimated by using a forward difference $\partial p_b / \partial x = \Delta p_b / \Delta x$. The horizontal density gradient term can be written as

$$\frac{g}{\rho_0 H} \int_{-h}^{\eta} \int_{-h}^z \frac{\partial \rho'}{\partial x} dz' dz = \frac{f}{H} \int_{-h}^{\eta} v_g(z) dz,$$

where

$$v_g(z) = \frac{g}{\rho_0 f} \int_{-h}^z \frac{\partial \rho'}{\partial x} dz'$$

is the baroclinic geostrophic velocity relative to the bottom. This term can be estimated for each cruise when CTD stations are available near the mooring sites. Time series of bottom density anomalies ρ'_h at adjacent moorings are averaged to form a new time series of bottom density at the mid-point. For station pair EC5–EC4, EC4–NA1 and CM4–EC1, the bottom slope $\partial h/\partial x$ is 0.5×10^{-3} , 0.6×10^{-3} , 1.7×10^{-3} , respectively. The bottom buoyancy term can be estimated once these two variables are known. The wind stress is estimated using a neutral drag law (Large and Pond, 1981), and the across-shelf component of bottom stress is parameterized by the quadratic form $\tau_b^x = \rho_0 C_D u_b \sqrt{u_b^2 + v_b^2}$, where u_b and v_b are the near bottom velocity components and C_D is a drag coefficient, taken to be 2.5×10^{-3} (to be explained in Section 7).

4.2. Across-shelf momentum balance on the inner shelf

Two diagnostic periods are considered, one for the full record length and the other for the period from February 2001 to March 2002, when the bottom pressure records at both EC4 and EC5 had minimal trends yielding the best quality data subset collected among the deployments.

4.2.1. Momentum balance on the inner shelf with the best quality data set

Diagnostic time series of all the across-shelf momentum terms during the February 2001–March 2002 period are shown in Fig. 2. The relative magnitude of each term may be measured by the standard deviations (Table 2). The standard deviations of the Coriolis and bottom pressure gradient terms are much larger than those of the other terms, suggesting that the across-shelf momentum balance is predominantly geostrophic. This is supported by the high visual correlation between these two terms (Fig. 2a) and by coherence (Fig. 3), which is significant with nearly zero phase over the frequency band 0.05–0.5 cpd.

The standard deviation of the wind stress term is about 0.65 that of the Coriolis term, and the maximum value of the wind stress term has the same magnitude as those of the Coriolis and bottom pressure gradient terms. To compare the wind stress term to the ageostrophic residual, we subtract the bottom pressure gradient term from the Coriolis term (Fig. 2b). This ageostrophic momentum term

visually resembles the wind stress term, and a coherence analysis (Fig. 4) demonstrates that the ageostrophic momentum residual can be largely accounted for by the wind stress.

That the across-shelf wind stress may play an important role in the momentum balance is evident in the July 22–24, 2001 event. The wind stress term has a value of $26 \times 10^{-6} \text{ m s}^{-2}$ (Fig. 2b), relative to the bottom pressure gradient term of $-38 \times 10^{-6} \text{ m s}^{-2}$ and the Coriolis term of $-19 \times 10^{-6} \text{ m s}^{-2}$ (Fig. 2a). Thus, the offshore bottom pressure gradient is maintained primarily by the onshore wind stress and secondarily by the Coriolis term, consistent with the Li and Weisberg (1999a, b) findings on the importance of the across-shelf wind stress in their numerical model diagnoses. More recently, the importance of the across-shelf winds as a mechanism for across-shelf transport within the friction-dominated inner shelf was also shown by Tilburg (2003) in a series of two-dimensional simulations.

The remaining terms of diminishing importance are the bottom buoyancy, the bottom stress, and the local acceleration. The standard deviation of the bottom buoyancy term is 0.29 that of the Coriolis term, and both the bottom friction and the local acceleration terms are an order of magnitude smaller than the Coriolis term.

A residual term is computed by summing all the momentum terms except the horizontal density gradient term (Fig. 2d). If the errors were negligible, the residual term should be accounted for by the horizontal density gradient term. However, the range of the density gradient term estimated from the monthly hydrographic data set (Table 3) is much smaller than that of the residual time series, showing that the remaining momentum residual is due to errors rather than the small density gradient term at this shallow (15 m) site (Fig. 5).

Time domain correlation (C) and regression (R) coefficients provide an alternate method for examining the contribution of each term to the across-shelf momentum balance. These are given between the bottom pressure gradient term and sums of the other terms in Table 4. The values of C and R between the bottom pressure gradient and the Coriolis terms are 0.81 (significant at 95% confidence level) and 0.61, respectively, and when the wind stress is included, C and R increase significantly to 0.93 and 0.88, respectively.

In Eq. (5) the LHS (the accelerations) may be regarded as responses to the RHS (the forcing

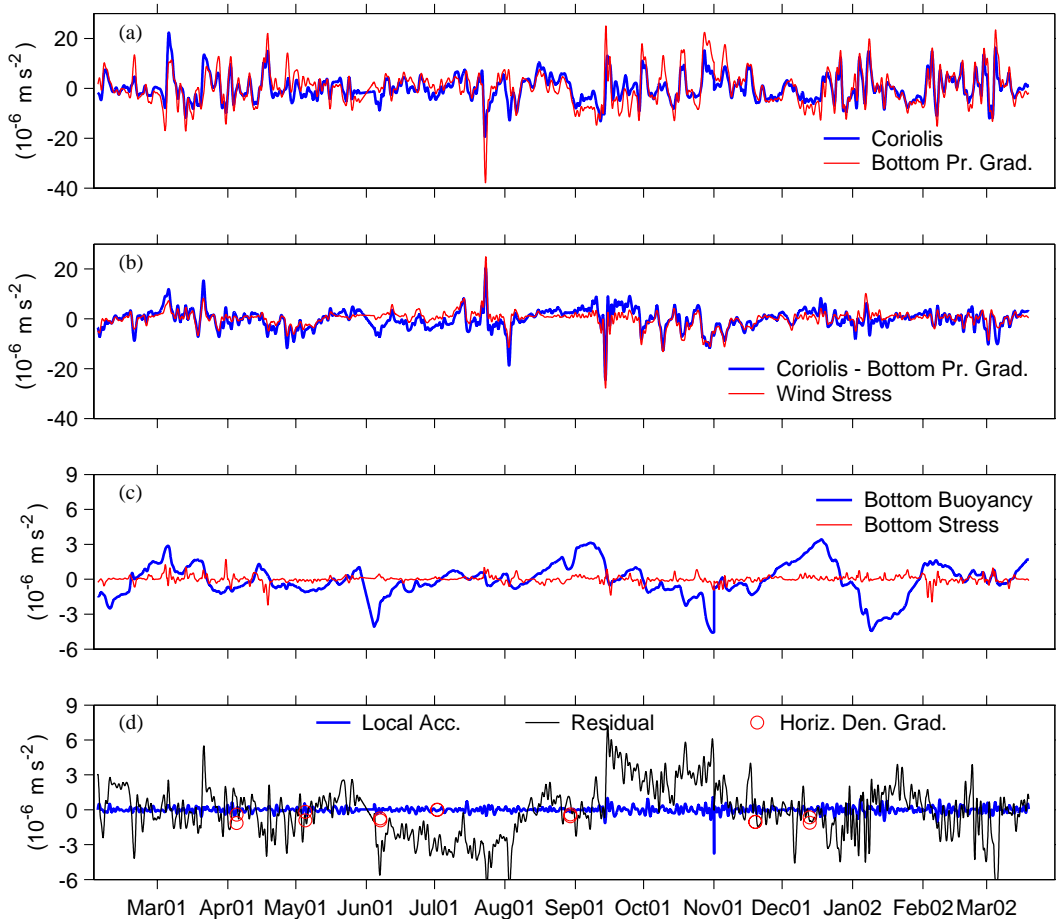


Fig. 2. Across-shelf momentum balance at 15 m site between the inner-shelf moorings EC4 and EC5 from February 2001 to March 2002. Note the scales of the vertical axes differ in different panels for the large and small terms: (a) The Coriolis vs. the bottom pressure gradient terms; (b) the ageostrophic residual between the Coriolis and the bottom pressure gradient terms vs. the wind stress term; (c) the bottom buoyancy and the bottom stress terms; and (d) the local acceleration term, the residual of the momentum terms except the horizontal density gradient term vs. the horizontal density gradient term calculated from the CTD data.

Table 2

Maximum, minimum values and standard deviations (σ) of the terms in the across-shelf momentum balance (units in 10^{-6} m s^{-2})

		$\frac{\partial \bar{u}}{\partial t}$	$-f\bar{v}$	$-\frac{1}{\rho_0} \frac{\partial p_b}{\partial x}$	$\frac{g\rho'_h}{\rho_0} \frac{\partial h}{\partial x}$	$\frac{\tau_s^x}{\rho_0 H}$	$-\frac{\tau_b^x}{\rho_0 H}$	Residual
EC4–EC5 (15 m) (best quality)	Max	1.08	22.34	24.97	3.42	24.92	1.70	7.21
	Min	−3.77	−19.44	−37.88	−4.60	−27.79	−2.21	−6.85
	σ	0.23	5.00	6.66	1.45	3.23	0.29	2.15
EC4–EC5 (15 m)	σ	0.20	4.51	6.17	0.96	2.60	0.24	2.76
NA1–EC4 (23 m)	σ	0.27	4.26	5.63	0.97	1.64	0.22	3.46
EC1–CM4 (126 m)	σ	0.42	5.81	5.24	1.86	0.36	0.06	5.23

functions of pressure gradient and friction terms) as shown in Fig. 6. Visually, the acceleration term is dominated by the pressure gradient term and complemented by the friction term. To quantify how much of the variance is accounted for by these

forcing terms, a two-input/one-output multiple coherence model is employed (Bendat and Pierson, 1986). In this statistical model, $x_1(t)$ (pressure gradient term) and $x_2(t)$ (friction term) are two random input variables, and $y(t)$ (acceleration term)

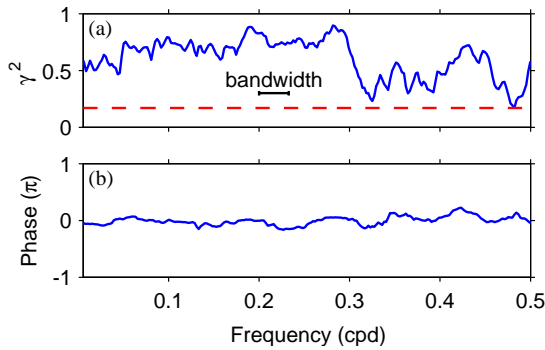


Fig. 3. Cross-spectral analysis between the Coriolis and the bottom pressure gradient terms in the across-shelf momentum equations for the 15m site between moorings EC4–EC5, February 2001 to March 2002 (the degrees of freedom is measured as 27): (a) coherence squared (dashed line shows 90% significance level); and (b) phase normalized by π .

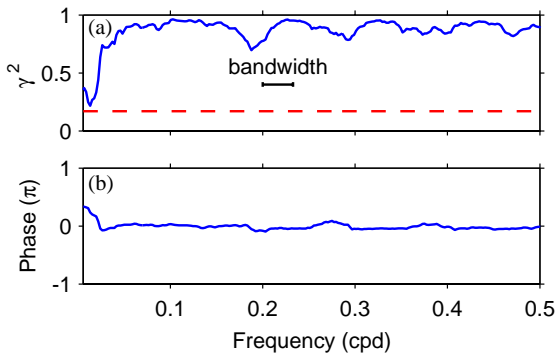


Fig. 4. Same as Fig. 3 except for the wind stress term and the ageostrophic momentum, which is defined as the difference between the Coriolis and the bottom pressure gradient terms.

Table 3

Ranges of the horizontal density gradient term estimated from monthly CTD data (units in 10^{-6} m s^{-2})

Density term	EC4–EC5 (15 m)	NA1–EC4 (22.5 m)	EC1–CM4 (126 m)
Maximum	1.7	1.5	24.9
Minimum	–1.9	–1.8	–8.7

is the single random output. The Fourier transform $Y(f)$ of the output is given by

$$Y(f) = H_1(f)X_1(f) + H_2(f)X_2(f) + N(f),$$

where H_1 and H_2 are the transfer functions between x_1 , y , and x_2 , y , respectively, calculated with the recognition that x_1 and x_2 may themselves be correlated. $N(f)$ is the Fourier transform of the

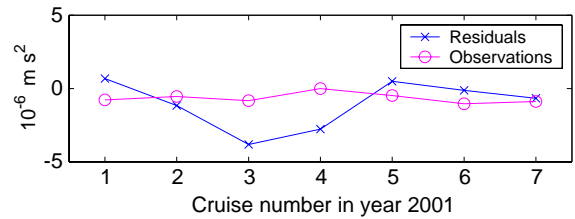


Fig. 5. Comparison of the across-shelf momentum residual and the density gradient terms estimated from the CTD observations.

uncorrelated noise input, and the output is the inverse Fourier transform of $Y(f)$.

The ordinary coherence between each input and the output, and between the two inputs are shown as a function of frequency (Fig. 7a). Input 1 is highly coherent with the output over the synoptic weather band (0.05–0.5 cpd), wherein the two inputs are also mutually coherent. The partial coherences for the conditioned input and output variables (by removing the effects of one of the inputs) are higher than the ordinary coherence counterparts, with the pressure gradient values larger than friction values (Fig. 7b). The multiple coherence gives the combined effects (Fig. 7c), and this is about 0.95 over the synoptic weather band. Thus, the combined pressure gradient and friction terms account for 95% of the acceleration variance. We also see that the amplitude of the transfer function H_1 is nearly 1, and which H_2 has larger variation (also nearly 1) (Fig. 7d), and the phases between the forcing terms and the response term are close to zero (Fig. 7e). These findings confirm the validity of the diagnostic equation over the synoptic weather band.

4.2.2. Across-shelf momentum balance on the inner WFS with the full-length records

The momentum terms are also estimated using the full-length records. The standard deviations of the individual momentum terms for the station pairs EC4–EC5 and NA1–EC4 are listed in bottom rows in Table 2. The standard deviations of the individual terms have similar magnitudes as the corresponding terms in Section 4.2.1 calculation for EC4–EC5, except for the residual term, which is larger due to longer record length and increased pressure gradient errors. Correlation and regression analyses are performed as in Section 4.2.1 (Table 4), and the same qualitative conclusions are drawn.

The balance for station pair NA1–EC4 is degraded from that of EC4–EC5. This is likely due to the different distance (Δx) in the finite

Table 4
Correlation and regression analyses of the across-shelf momentum terms

$x(t)$ versus $y(t)$	EC4–EC5 (best qual.)		EC4–EC5 (15 m)		NA1–EC4 (23 m)		EC1–CM4 (126 m)	
	C	R	C	R	C	R	C	R
$-\frac{1}{\rho} \frac{\partial p_h}{\partial x}$ vs. $-f\bar{v}$	0.81	0.61	0.75	0.55	0.73	0.55	0.58	0.64
$-\frac{1}{\rho} \frac{\partial p_h}{\partial x}$ vs. $-f\bar{v} - \frac{\tau_x^x}{\rho_0 H}$	0.93	0.88	0.88	0.77	0.78	0.67	0.59	0.65
$-\frac{1}{\rho} \frac{\partial p_h}{\partial x}$ vs. $-f\bar{v} - \frac{\tau_x^x}{\rho_0 H} - \frac{g\rho'_h}{\rho_0} \frac{\partial h}{\partial x}$	0.95	0.95	0.89	0.80	0.79	0.71	0.62	0.76
$-\frac{1}{\rho} \frac{\partial p_h}{\partial x}$ vs. $-f\bar{v} - \frac{\tau_x^x}{\rho_0 H} - \frac{g\rho'_h}{\rho_0} \frac{\partial h}{\partial x} + \frac{\tau_h^x}{\rho_0 H}$	0.95	0.97	0.89	0.82	0.79	0.73	0.62	0.76
$-\frac{1}{\rho} \frac{\partial p_h}{\partial x}$ vs. $-f\bar{v} - \frac{\tau_x^x}{\rho_0 H} - \frac{g\rho'_h}{\rho_0} \frac{\partial h}{\partial x} + \frac{\tau_h^x}{\rho_0 H} + \frac{\partial \bar{u}}{\partial t}$	0.95	0.98	0.89	0.83	0.80	0.74	0.62	0.76

C : correlation coefficient, all significant at 90% level; R : regression coefficient.

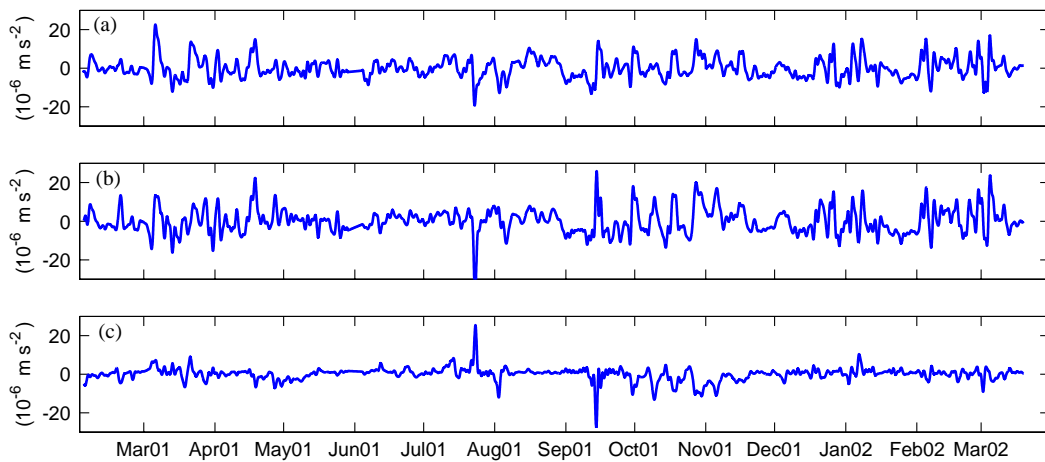


Fig. 6. Comparison of the across-shelf momentum terms at 15m site between moorings EC4–EC5, February 2001–March 2002: (a) acceleration (a sum of the local acceleration and the Coriolis terms); (b) pressure gradient (a sum of the bottom pressure gradient term and the bottom buoyancy term); and (c) friction (a sum of the wind stress and bottom stress terms).

difference estimate of the bottom pressure gradient [the distance between NA1 and EC4 (~ 10 km) is half that of EC4/EC5 (~ 20 km)]. The smaller denominator may amplify the finite difference errors of the bottom pressure gradient. Also, the deeper water location may increase the residual due to the baroclinic effect.

4.3. Across-shelf momentum balance on the outer shelf

The outer shelf moorings EC1 and CM4 share the common observation period from 25 June 2000 to 25 June 2001. Like those of the inner shelf, the standard deviations of the Coriolis and the bottom pressure gradient terms are the largest (Table 2); in contrast with the inner shelf, the standard deviation of the residual term is as large as the bottom pressure gradient term, and this may be due to

increased baroclinic effects with deeper water. From Table 3, the horizontal density gradient term estimated from the monthly hydrography near station pair EC1–CM4 ranges from -8.7×10^{-6} to $24.9 \times 10^{-6} \text{ m s}^{-2}$, with magnitudes similar to the Coriolis and bottom pressure gradient terms (Fig. 8). Thus, the horizontal density gradient term plays a significant role in the across-shelf momentum balance on the outer WFS. Also, the standard deviation of the bottom buoyancy term ($1.86 \times 10^{-6} \text{ m s}^{-2}$) is 0.32 that of the Coriolis term and is larger than that on the inner shelf.

The correlation and regression analyses for station pair EC1–CM4 (Table 4) are similar to those of the inner shelf station pairs in that each term makes a positive contribution to the momentum balance; the correlation and regression coefficients are much smaller than those of the inner shelf station pairs, which again is likely due to the

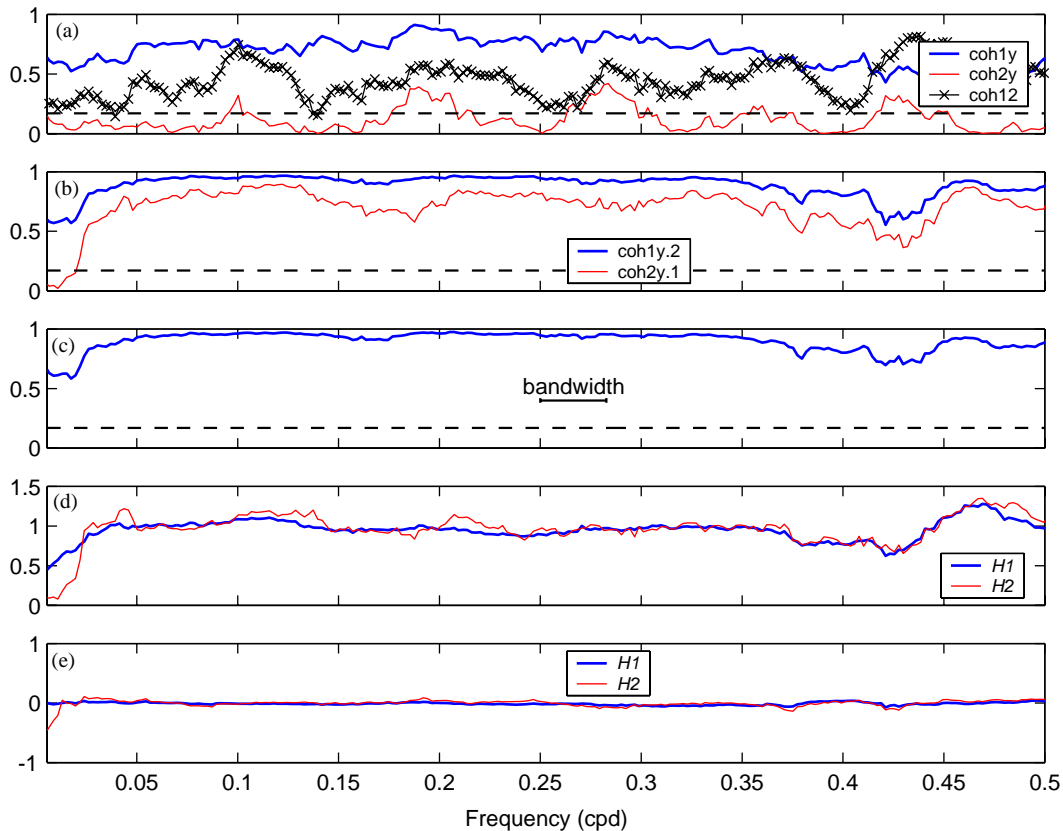


Fig. 7. Multiple coherence analysis from the two-input/one-output statistic model with the three terms defined in Fig. 6. Inputs: (1) the pressure gradient term; and (2) the friction term; Output: the acceleration term. (a) Ordinary coherence (dashed line is 90% significance level, the same in (b) and (c)); (b) partial coherence; (c) multiple coherence; (d) amplitude of the transfer function; and (e) phase of the transfer function (unit in π).

horizontal density gradient term not included in the regression analyses.

A residual time series is formed after summing all the terms in Eq. (5) except the horizontal density gradient term (Fig. 8d). The horizontal density gradient term is superimposed as discrete open circles for each cruise. There are usually five CTD station pairs between moorings EC1 and CM4, so there are five values in each cruise to give a range of the density gradient term. The residual line passes through the circles in most cases, which indicates the residuals can be accounted for by the horizontal density gradient term.

The pressure gradient term is composed of the bottom pressure gradient, the horizontal density gradient and the bottom buoyancy terms; the latter two terms are directly related to density. Baroclinic adjustment to the currents plays an important role on the outer shelf, sometimes dominating. It is known that the circulation near the shelf break is often affected by the deep ocean. For instance,

during June–July 2000, the Loop Current intruded onto the shelf slope (He and Weisberg, 2003), and mooring EC1 recorded strong currents during this event. These findings help to define what is commonly referred to as the mid and outer shelves. The outer shelf is the region where deep ocean effects are readily observed in the vicinity of the shelf slope and shelf break. By virtue of the Taylor–Proudman theorem, however, the shoreward penetration of these outer shelf responses to deep ocean forcing are limited, so the mid-shelf is the region between the outer shelf and the inner shelf, assuming that the shelf is wide enough to draw such demarcation.

5. Along-shelf momentum balance

5.1. Estimation of terms

The local acceleration, the Coriolis, and the wind stress terms can be estimated as in Section 4.1. Our

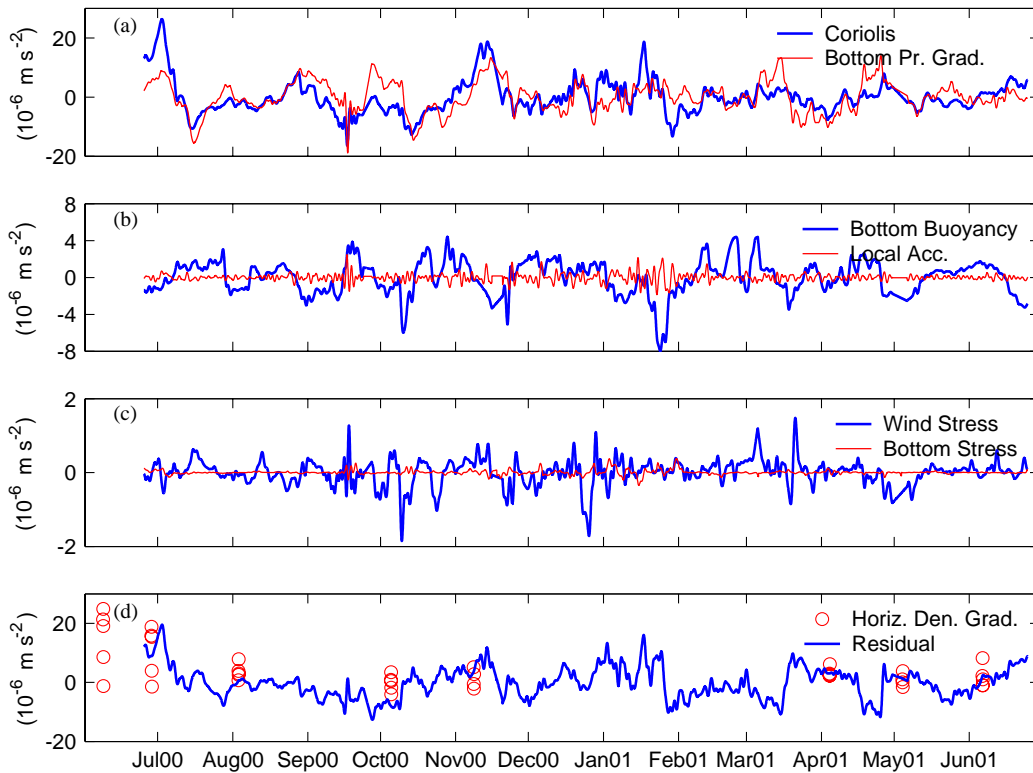


Fig. 8. Across-shelf momentum terms between the outer shelf moorings EC1 and CM4 (126 m) from June 2000 to July 2001. Note the scales of the vertical axes differ in different panels for the large and small terms: (a) the Coriolis vs. the bottom pressure gradient terms; (b) the bottom buoyancy and the local acceleration terms; (c) the wind stress and the bottom stress terms; and (d) the residual of the momentum terms except the horizontal density gradient term vs. the horizontal density gradient term calculated from the CTD data.

data are insufficient to estimate the vertical structure of the along-shelf pressure gradient, but since EC5 and EC6 are shallow (10 m) sites, a constant pressure gradient is assumed throughout the water column. The pressure gradient is estimated in two ways: (1) using bottom pressure at EC5 and EC6, separated along the shelf by 108 km; and (2) using coastal sea level at Clearwater and Naples, separated by 229 km. The bottom stress may be parameterized either in a quadratic form, $\tau_b^y = \rho_0 C_D v_b \sqrt{u_b^2 + v_b^2}$, or in a linear form, $\tau_b^y = \rho_0 r \bar{v}$, where r is a resistance coefficient. We take $r = 5 \times 10^{-4} \text{ m s}^{-1}$ for the bottom stress estimation at the 10 m sites (to be explained in Section 7).

5.2. Standard deviations

The standard deviations of the along-shelf momentum terms from the EC5 and EC6 10 m sites show that the wind stress term is the largest one (Table 5), followed by the bottom friction, the

pressure gradient, the local acceleration, and the Coriolis terms. The standard deviations of the wind stress and bottom friction terms decrease, while that of the Coriolis term increases, with the increasing water depth because the currents are more isotropic and the across-shelf velocity component is larger in the deeper sites. The wind stress, the bottom friction, and the Coriolis terms all have equal magnitude around a depth of 25–30 m. Further offshore, the standard deviation of the Coriolis term becomes larger than those of the wind stress and the bottom friction terms. At the two 10 m sites, the standard deviation of the residual term is even larger than those of the three small terms. The residual may be attributed to observational and diagnostic errors, although it could also be due to the advection terms that are not estimated.

5.3. Correlation and regression analyses

We first assume that the along-shelf wind stress and pressure gradient are the two forcing factors,

Table 5

Standard deviations of the terms in the along-shelf momentum balance (units in 10^{-6} m s^{-2})

Station & water depth	Data length (h)	Standard deviations					Residual
		$\frac{\partial \bar{u}}{\partial t}$	$f\bar{u}$	$-g\frac{\partial h}{\partial y}$	$\frac{\tau_s^y}{\rho_0 H}$	$-\frac{\tau_b^y}{\rho_0 H}$	
EC5 (10 m)	32,272	1.11	0.58	1.95	4.71	3.79 (2.54)	2.81
EC6 (10 m)	25,578	1.19	0.68	1.88	4.68	3.73 (3.59)	2.53
EC4 (20 m)	32,274	0.99	1.22	—	2.35	1.85 (1.27)	—
NA1 (25 m)	27,336	0.97	1.50	—	1.84	1.61 (0.96)	—
NA2 (25 m)	28,227	1.09	1.47	—	1.90	1.80 (1.12)	—
NA3 (25 m)	26,377	0.94	1.60	—	1.83	1.55 (1.33)	—
EC3 (30 m)	26,951	1.02	1.69	—	1.54	1.53 (1.07)	—
EC2 (50 m)	18,472	0.85	2.77	—	0.99	0.76 (0.46)	—
CM4 (78 m)	10,638	0.73	4.06	—	0.61	0.64 (0.58)	—
EC1 (162 m)	8759	0.60	2.91	—	0.30	0.38 (0.30)	—

The bottom stress term values in the parentheses are calculated with quadratic parameterization ($C_D = 3.2 \times 10^{-3}$).

and the summation of the other momentum terms is the response. Correlation and regression coefficients between the forcing and the response are calculated for each of these summations (Table 6). When the bottom stress term is considered to be the only response, C is significantly high. The local acceleration term contributes positively to the along-shelf momentum balance, while the Coriolis term degrades the balance. We next consider the wind stress to be the only forcing function, with the other terms taken as the responses (Table 7). C and R between the bottom friction and the wind stress terms are higher than those between the pressure gradient and the wind stress terms. When both the bottom friction and the pressure gradient terms are considered as the responses, C and R increase significantly. As a response to the wind stress, the pressure gradient is secondary to the bottom friction. Again, the local acceleration term contributes positively to the balance, but the Coriolis term degrades the results. Similar findings are given by Hickey et al. (2003).

5.4. Multiple coherence analysis

Similar to the across-shelf direction we also apply a frequency domain analysis. The two inputs are the along-shelf wind stress and the pressure gradient terms. The output is set to be a sum of the local acceleration, the Coriolis and the bottom stress terms; all derived from the moored velocity records. Velocities from moorings EC5 and EC6 are averaged to form a new velocity time series for the 10 m isobath. Data from 1 September 1999 to 23

Table 6

Correlation and regression analyses of the along-shelf momentum balance at 10 m sites

Forcing and response	EC5		EC6	
	C	R	C	R
$\frac{\tau_s^y}{\rho_0 H} - g\frac{\partial h}{\partial y}$ vs. $\frac{\tau_b^y}{\rho_0 H}$	0.68	0.71	0.72	0.73
$\frac{\tau_s^y}{\rho_0 H} - g\frac{\partial h}{\partial y}$ vs. $\frac{\tau_b^y}{\rho_0 H} + \frac{\partial \bar{u}}{\partial t}$	0.74	0.80	0.77	0.81
$\frac{\tau_s^y}{\rho_0 H} - g\frac{\partial h}{\partial y}$ vs. $\frac{\tau_b^y}{\rho_0 H} + f\bar{u}$	0.68	0.71	0.73	0.75
$\frac{\tau_s^y}{\rho_0 H} - g\frac{\partial h}{\partial y}$ vs. $\frac{\tau_b^y}{\rho_0 H} + f\bar{u} + \frac{\partial \bar{u}}{\partial t}$	0.73	0.80	0.78	0.83

C : correlation coefficient, all significant at 90% level; R : regression coefficient.

Table 7

Correlation and regression analyses of the along-shelf momentum balance at 10 m sites

Forcing and response	EC5		EC6	
	C	R	C	R
$\frac{\tau_s^y}{\rho_0 H}$ vs. $\frac{\tau_b^y}{\rho_0 H}$	0.73	0.59	0.75	0.59
$\frac{\tau_s^y}{\rho_0 H}$ vs. $g\frac{\partial h}{\partial y}$	0.68	0.28	0.67	0.27
$\frac{\tau_s^y}{\rho_0 H}$ vs. $\frac{\tau_b^y}{\rho_0 H} + g\frac{\partial h}{\partial y}$	0.82	0.87	0.83	0.86
$\frac{\tau_s^y}{\rho_0 H}$ vs. $\frac{\tau_b^y}{\rho_0 H} + g\frac{\partial h}{\partial y} - f\bar{u}$	0.81	0.87	0.84	0.88
$\frac{\tau_s^y}{\rho_0 H}$ vs. $\frac{\tau_b^y}{\rho_0 H} + g\frac{\partial h}{\partial y} - \frac{\partial \bar{u}}{\partial t}$	0.85	0.92	0.86	0.91
$\frac{\tau_s^y}{\rho_0 H}$ vs. $\frac{\tau_b^y}{\rho_0 H} + g\frac{\partial h}{\partial y} - f\bar{u} - \frac{\partial \bar{u}}{\partial t}$	0.84	0.91	0.87	0.92

C : correlation coefficient, all significant at 90% level; R : regression coefficient.

August 2001 are used, and the results are shown in Fig. 9.

The pressure gradient input (1) has lower coherence with the output than the wind stress term input (2); but the coherence between the two inputs is high over the synoptic weather frequency band. The partial coherence between the conditioned input 2 and the output is high, whereas the partial coherence between the conditioned input 1 and the output is smaller. There is a high degree of multiple coherence between the two inputs and the output over the synoptic weather band, with an average value of 0.75. That is to say, over 75% of the “current” variance may be accounted for by the wind stress and pressure gradient terms.

5.5. A linear nowcast model for along-shelf velocity

The foregoing statistical results justify the application of a simple dynamic model to nowcast the

along-shelf velocity. Following Lentz and Winant (1986) and Hickey et al. (2003), along-shelf wind stress and pressure gradient are used to drive a depth-averaged one-dimensional linear model of the along-shelf currents. Assuming that the Coriolis term is negligible and that the bottom stress is a linear function of depth-averaged velocity $\tau_b^y = \rho_0 r \bar{v}$, Eq. (3b), upon integration in time, provides the depth-averaged along-shelf velocity as

$$\bar{v}(t) = \bar{v}_0 \exp\left(-\frac{rt}{H}\right) + \int_0^t \frac{\tau_s^y}{\rho_0 H} \exp\left[-\frac{r(t-t')}{H}\right] dt' - \int_0^t \frac{1}{\rho_0} \left\langle \frac{\partial p}{\partial y} \right\rangle \exp\left[-\frac{r(t-t')}{H}\right] dt', \quad (6)$$

where $\bar{v}_0 = \bar{v}(0)$ is the initial condition. H/r is the frictional adjustment time, and with $r = 5 \times 10^{-4} \text{ ms}^{-1}$ (as in Lentz and Winant, 1986; Hickey et al., 2003), and $H = 10 \text{ m}$, the adjustment time is about 6 h. Thus, the effective integration time is on the order of a pendular day, and the initial condition

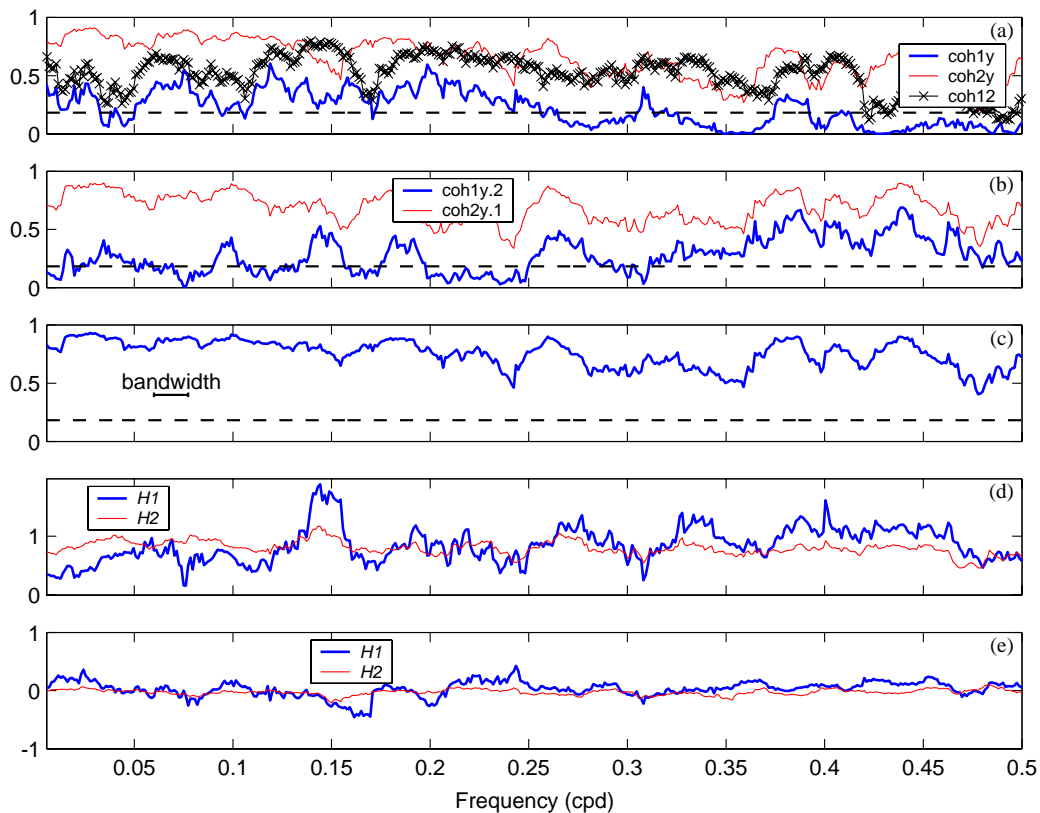


Fig. 9. Multiple coherence analysis with the two-input/one-output statistic model for the along-shelf momentum balance at the 10 m site between moorings EC5–EC6. Inputs: (1) the along-shelf sea level gradient term, and (2) the along-shelf wind stress term; Output: a sum of the local acceleration, the Coriolis, and the bottom stress terms. (a) Ordinary coherence (dashed line is 90% significance level, the same in (b) and (c)); (b) partial coherence; (c) multiple coherence; (d) amplitude of the transfer function; and (e) phase of the transfer function (units in π).

\bar{v}_0 is relatively unimportant. Since the model is linear, estimates can be made for the wind stress and pressure gradient either alone, or together.

The along-shelf wind stress for the inner shelf, bottom pressure at moorings EC5 and EC6, and sea level records at the Clearwater and Naples coastal stations from 15 December 2000 through 30 April 2001 are used to nowcast the depth-averaged along-shelf currents at the 10 m isobath. The model results are compared with observations in Fig. 10. The wind stress estimated currents are highly correlated with the observations, but they are overestimated in amplitude. The pressure gradient forced currents are weaker than those estimated by the wind stress, and they are negatively correlated with the observa-

tions. When the model is forced by wind stress and along-shelf bottom pressure gradient together, the estimated currents are closer to the observations. Thus, the along-shelf wind stress is the dominant driver, while the pressure gradient is complementary. Calculating the pressure gradient from coastal sea level (as opposed to bottom pressure) improves the results.

The along-shelf wind stress and the pressure gradient terms themselves are negatively correlated (correlation coefficient -0.67 to -0.68 , from Table 7). The high coherence between these two terms can also be seen from the previous multiple coherence analyses (Fig. 9a). Thus, the pressure gradient derives from the local wind, rather than

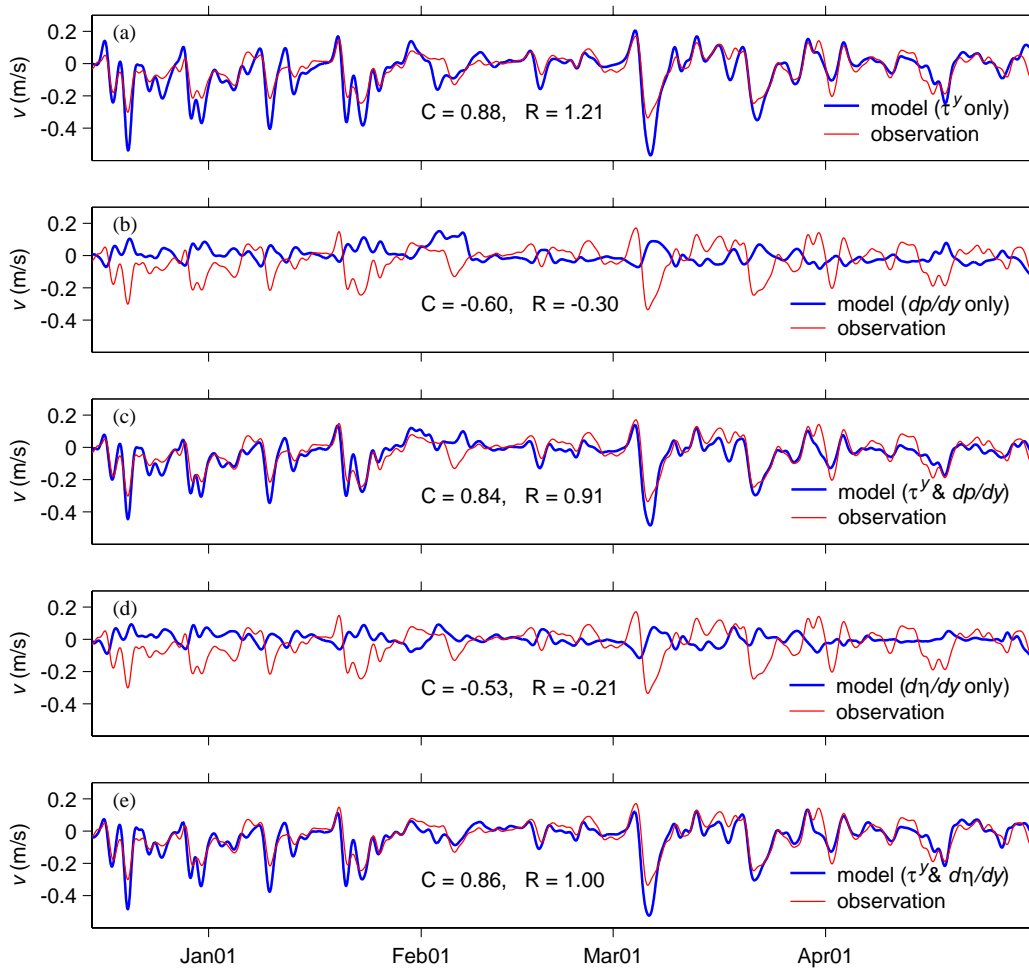


Fig. 10. Comparisons of the depth-averaged along-shelf velocity estimated with a linear nowcast model along the 10 m isobath and that from the observations at moorings EC5 and EC6 (C : correlation coefficient, R : regression coefficient, where $V_{\text{model}} = V_{\text{observation}} \times R + \text{constant}$, same in Fig. 11). (a) The model is forced by the along-shelf wind stress only; (b) the model is forced by the along-shelf bottom pressure gradient only, with the bottom pressure records from moorings EC5 and EC6; (c) the model is forced by both the along-shelf wind stress and the along-shelf bottom pressure gradient; (d) and (e) are the same as (b) and (c), respectively, except the along-shelf pressure gradient is approximated by the coastal sea level gradient between Clearwater and Naples.

remotely. From this point of view, the WFS is quite different from either the Pacific Northwest Shelf (Hickey, 1984) or the central Southern California Bight (Hickey et al., 2003), where the along-shelf pressure gradient is generated primarily non-locally and the pressure gradient disturbances account for a much larger fraction of the along-shelf velocity variance than the local wind stress.

The interpretation on the WFS is relatively straightforward. By a classical Ekman-geostrophic spin-up the along-shelf wind generates an along-shelf current over the course of a pendular day (e.g., Weisberg et al., 2000) with bottom stress tending to balance the wind stress. However, owing to the full three-dimensional nature of the response an along-shelf pressure gradient also develops that partially counteracts the wind stress. Without provision for the pressure gradient the along-shelf wind response is overestimated. These results are essentially as shown in the model study of Li and Weisberg (1999b).

6. Applications of the momentum balances

From the foregoing considerations, is it possible to estimate currents from readily observed variables such as wind and coastal sea level and to provide offshore sea surface height variation from independently observed currents?

6.1. Nowcast the depth-averaged along-shelf currents

As already known, the first three dominant terms in the across-shelf momentum balances over the inner shelf are the Coriolis, the pressure gradient, and the wind stress terms. Thus, the depth-averaged along-shelf velocity may also be expressed as

$$\bar{v} = \frac{1}{\rho_0 f} \frac{\partial p_b}{\partial x} - \frac{\tau_s^x}{\rho_0 f H}. \quad (7)$$

Based on the bottom pressure data at moorings EC4 and EC5, wind on the inner shelf, and coastal sea level at Naples and Clearwater, the along-shelf velocity is estimated using Eqs. (6) and (7), respectively. The resistance coefficient is set to be $3.5 \times 10^{-4} \text{ m s}^{-1}$, and the coastal sea level gradient is down-scaled by a factor of 0.7 to get the along-shelf pressure gradient at the 15 m site. While the along-shelf wind stress tends to over-predict the along-shelf current, especially during strong wind events (Fig. 11a), the along-shelf pressure gradient helps to eliminate the offset between the estimates and the

observations (Fig. 11b). The across-shelf pressure gradient generally predicts the currents well except for some strong current events (Fig. 11c), while the across-shelf wind stress improves the current estimation at these peaks (Fig. 11d). At some peaks (for example, around early August 2001 and mid-September 2001), Eq. (6) overestimates, while Eq. (7) underestimates the velocity (Fig. 11b and d). An average between these two estimates gives a better nowcast result (Fig. 11e). During the spin-up period, the momentum from the wind stress is not fully exerted on the currents, thus the currents are overestimated if the wind stress is used to drive the along-shelf model (Eq. (6)). Similarly, the currents are underestimated by the across-shelf model (Eq. (7)) during the spin-up period. The real currents lie between these two estimates.

The down-scale factor of 0.7 is used to approximate the along-shelf pressure gradient at the 15 m isobath from the coastal sea level. Hickey (1984) also used a value of 0.7–0.8 on the Pacific Northwest Shelf. As a test of sensitivity we also tried values of 0.9 and 0.5. With 0.9, the estimated currents are weaker [$C = 0.76$, $R = 0.88$ in Fig. 11(b)], whereas with 0.5, they are stronger [$C = 0.82$, $R = 1.07$ in Fig. 11(b)]. Based on regression coefficient the 0.7 value seems to be approximately correct.

6.2. Estimate the across-shelf pressure gradient

By rearranging Eq. (7), we have $\partial p_b / \partial x = \rho_0 f \bar{v} + \tau_s^x / H$, and the across-shelf pressure gradient may be estimated from the depth-averaged along-shelf currents and the across-shelf wind stress. The inner-shelf winds and coastal sea level at Clearwater and Naples are used to nowcast the depth-averaged along-shelf currents at the 15 m site again using Eq. (6) (Fig. 11b). Both the estimated currents and the observed across-shelf wind stress are further used to calculate the across-shelf pressure gradient. The currents underestimate the across-shelf pressure gradient (Fig. 11f); the across-shelf wind stress alone explains a part of the across-shelf pressure gradient only during certain major events (Fig. 11g)). Together, the currents and the wind stress reproduce the across-shelf pressure gradient quite well (Fig. 11(h)). Over the largely barotropic inner shelf, the sea level gradient approximates the bottom pressure gradient. Thus, the wind and coastal sea level data provide an estimate of the offshore sea surface height variation.

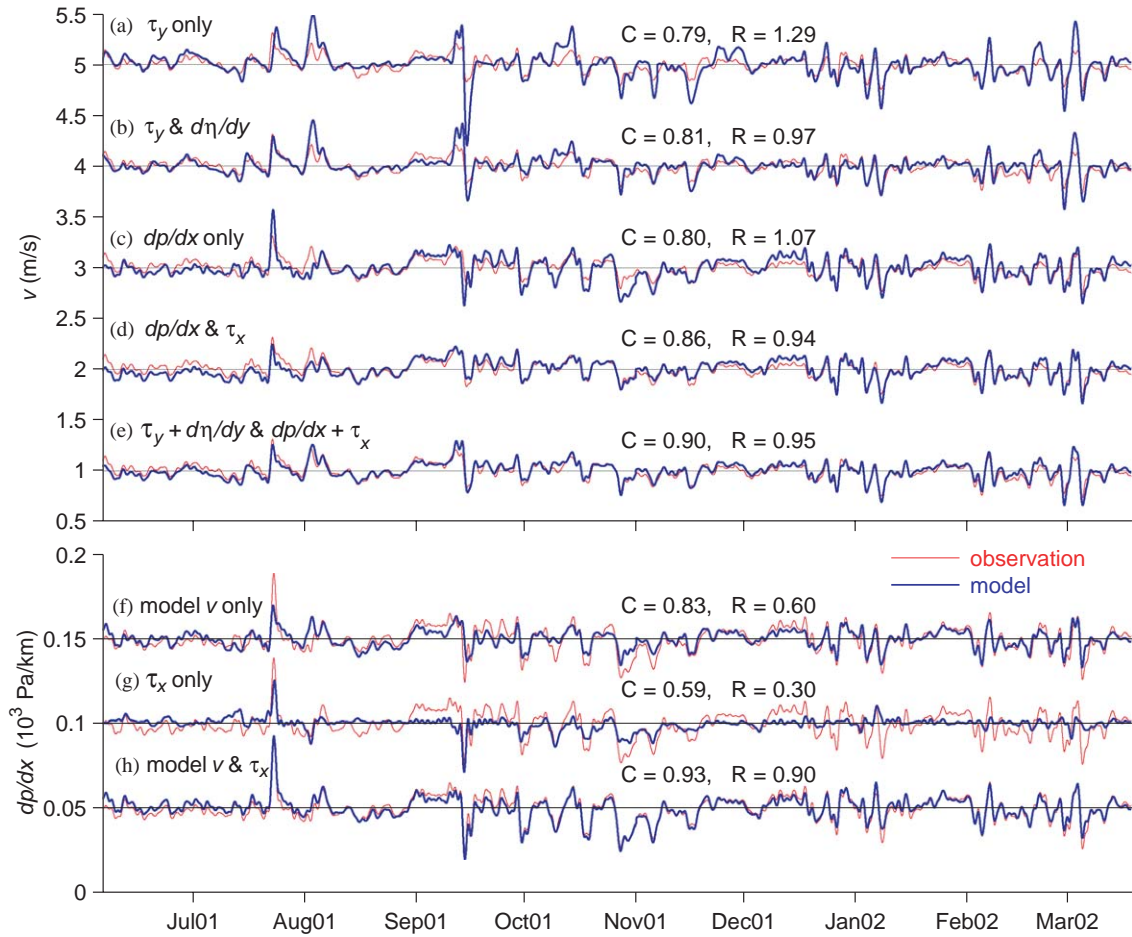


Fig. 11. Application of the momentum balances at 15m site. Upper panel: stack plot of the depth-averaged along-shelf currents from observation (thin lines) vs. those (thick lines) estimated from the along-shelf wind stress τ_y alone (a) and with the along-shelf sea level gradient $d\eta/dy$ together (b), or from the across-shelf pressure gradient dp/dx alone (c) and with the across-shelf wind stress τ_x together (d); an average of (b) and (d) gives a better result in (e). Lower panel: stack plot of the across-shelf sea level (pressure) gradient from observations (thin lines) vs. those (thick lines) estimated from the along-shelf currents (modelled from τ_y and $d\eta/dy$) and the across-shelf wind stress τ_x (C: correlation coefficient, R: regression coefficient).

7. Estimate of bottom drag and resistance coefficients

The bottom drag coefficient C_D may be estimated by equating the bottom stress term to the residual of the other momentum terms, using the near bottom velocity to fit the bottom stress term. If we set $x(t) = v_b \sqrt{u_b^2 + v_b^2} / H$ and

$$y(t) = \frac{\partial \bar{v}}{\partial t} + f\bar{u} + g\frac{\partial \eta}{\partial y} - \frac{\tau_s^y}{\rho_0 H},$$

a regression coefficient C_D may be estimated from a least-squares fit of the linear system $y(t) = C_D x(t) + b$, where b is a constant. Based on the velocity data

obtained at mooring EC5, C_D is estimated to be 3.2×10^{-3} ; however, velocity data at EC6 yields a C_D of 2.1×10^{-3} . As an alternate method, C_D may be determined via an empirical search. By using different C_D values, and thus different estimates of the bottom stress term, the along-shelf momentum balance is different. Optimal C_D values may be obtained from the momentum balance in such a way that the C_D either: (a) minimizes the mean imbalance squared; (b) maximizes the correlation coefficient between the along-shelf wind stress term (the leading term) and the summation of the other terms; or (c) optimizes the regression between these two terms by setting the regression coefficient equal to 1. Using the velocity data at the 10m sites

(moorings EC5 and EC6) to perform the empirical search yields C_D ranges of 2×10^{-3} – 4×10^{-3} (Fig. 12). These values are close to those in Feddersen and Guza (2003). Numerical models on the WFS (Li and Weisberg, 1999a; He and Weisberg, 2002b; He et al., 2004) employing the Princeton Ocean Model of Blumberg and Mellor (1987) take the bottom drag coefficient as

$$C_D = \max \left\{ 2.5 \times 10^{-3}, \left[\frac{1}{k} \ln \left(\frac{1 + \sigma_b}{z_0/H} \right) \right]^{-2} \right\},$$

where k is the von Karman constant, z_0 is the bottom roughness length, σ_b is the σ value of the grid point next to the bottom, and H is the water depth. Except near shore, the C_D in these WFS model calculations is generally 2.5×10^{-3} .

A similar linear regression is made from the across-shelf momentum balance by assuming the density gradient term is negligible. Using the

EC4–EC5 data we arrive at a C_D value of 1.5×10^{-3} . This value is smaller than those from the along-shelf momentum balance. Since the residual of the much larger terms (the Coriolis and bottom pressure gradient) is likely more error prone, causing C_D to be underestimated. Thus, $C_D = 2.5 \times 10^{-3}$ is used for the across-shelf bottom stress estimation, for both the inner and outer shelf areas.

The resistance coefficient r may also be estimated. Again, by taking a linear regression of the along-shelf momentum terms, setting $x(t) = \bar{v}/H$ and keeping $y(t)$ the same, r is calculated as 4.1×10^{-4} and $4.3 \times 10^{-4} \text{ m s}^{-1}$, respectively, for the data from EC5 and EC6. If v_b is used instead of \bar{v} , these two r values become 3.4×10^{-4} and $3.6 \times 10^{-4} \text{ m s}^{-1}$. These values are larger than those (1×10^{-4} – $2 \times 10^{-4} \text{ m s}^{-1}$) estimated by Mitchum and Sturges (1982), but smaller than the value of $5 \times 10^{-4} \text{ m s}^{-1}$ used by Lentz and Winant (1986), Lentz et al. (1999), and Hickey et al. (2003). As before, empirical search is performed to obtain an optimal r . We run a series of model experiments as in Section 5.5 in which we vary r from 1×10^{-4} to $6 \times 10^{-4} \text{ m s}^{-1}$, the estimated along-shelf velocities are then compared with the observations. The r values corresponding to the minimum mean square error, the maximum correlation and a regression coefficient of 1 are regarded as the optimal estimates. For any r values larger than $2 \times 10^{-4} \text{ m s}^{-1}$ the mean squared error is small and the correlation is significantly high (Fig. 13); the optimal r value for the best regression coefficient is around $5 \times 10^{-4} \text{ m s}^{-1}$. Chuang and Wiseman (1983) used a wide range of r values (1 – $10 \times 10^{-4} \text{ m s}^{-1}$) in a one-dimensional model on the Louisiana and Texas Shelf. He and Weisberg (2002b) obtained r values of 0.6×10^{-4} – $6 \times 10^{-4} \text{ m s}^{-1}$ on the WFS with larger values near shore. Hickey et al. (2003) also found that a much better momentum balance is obtained if larger r value is used. Unless otherwise noted, the value of $5 \times 10^{-4} \text{ m s}^{-1}$ is used in the along-shelf bottom stress parameterization.

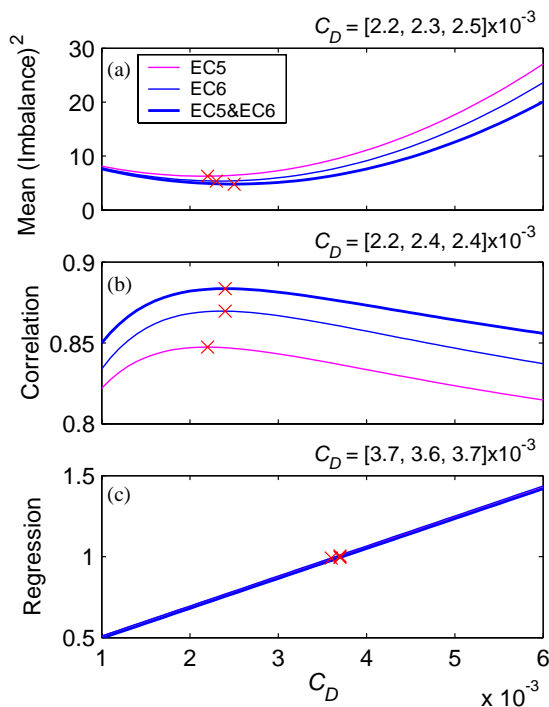


Fig. 12. Statistics of the along-shelf momentum terms at the 10 m sites as a function of the bottom drag coefficient C_D . The optimal C_D values may: (a) minimize the mean imbalance squared, where the imbalance is a sum of all the momentum terms; (b) maximize the correlation coefficient; and (c) optimize the regression coefficient (= 1) between the along-shelf wind stress and the sum of the other terms. Atop of each panel are the optimal C_D values estimated from the EC5 and EC6 data alone, and from an average of the EC5 and EC6 data.

8. Discussions

Errors in the momentum balances derive from the observations, the diagnostic calculations, and the simplified dynamics.

In calculating the depth-averaged currents we must integrate vertically and average horizontally. Data gaps near the surface and bottom must be

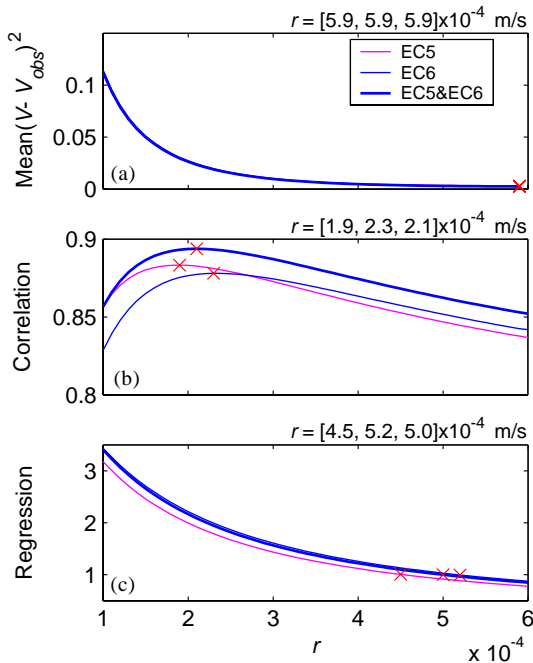


Fig. 13. Statistics of the estimated and observed depth-averaged along-shelf velocity at the 10m sites as a function of the bottom resistance coefficient r : (a) mean squared error; (b) correlation; and (c) regression coefficients. The r values estimated from the EC5 and EC6 data alone, and from an average of the EC5 and EC6 data are listed in the bracket on top of each panel.

considered. Experiments performed with either uniform, linear, or no extrapolation of velocity to the surface and bottom gave slightly different results. The case of no extrapolation, i.e., the average of available data only gave better results than an assumed vertical structure. Resolving the near bottom and near surface few meters of the water column would be beneficial in the future velocity observations. Experiments were also performed with different horizontal averaging with the best results obtained by a depth weighted average.

The major source of observational error is in the bottom pressure data. For example, with a distance $\Delta x = 20$ km, $f = 0.66 \times 10^{-4} \text{ s}^{-1}$ at the latitude of the WFS, $\rho_0 = 1023 \text{ kg m}^{-3}$, a bottom pressure error of 0.1 dbar (or 100 Pa) translates to an error of 7.3 cm s^{-1} in velocity according to the geostrophic relation $\Delta v = (\rho_0 f)^{-1} \Delta P_b / \Delta x$. Pressure accuracy was stated to be in 0.15% of full-scale range. But the linear trend (0.02–0.2 bar at moorings EC4, EC5 and EC6) is much larger than this. Wind and bottom stress parameterizations may also introduce errors. The bottom drag coefficient C_D and bottom

resistance coefficient r are not constant (Grant et al., 1984). Comparing these values used by various investigators is difficult (Winant and Beardsley, 1979; Grant et al., 1984). Moreover, nonlinear parameterizations are more accurate than linear parameterizations (Feddersen et al., 2000). Errors are also introduced when bottom temperature alone is used to infer bottom density. Additional density data are required to better estimate the baroclinic terms.

Advection terms do not appear in our diagnostic momentum equations. Thompson and Pugh (1986) show that advection is due to the subtidal flow and mean tidal advection. The Rossby number for the interior circulation is typically 10^{-2} and the subtidal advection can generally be ignored. These findings for the subtidal motions are consistent with the numerical model results of Li and Weisberg (1999a, b) where the advection terms were an order of magnitude smaller than the lead momentum balance terms. Rectification by tidal currents may be a factor where tidal currents are large. However, on the WFS, the tides are generally weak (He and Weisberg, 2002b), so their effect on the subtidal circulation is thought to be small.

Lentz et al. (1999) consider a wave radiation stress term in a momentum balance on the North Carolina inner shelf. Radiation stress is found to be important in the across-shelf momentum balance offshore of the surf zone, in depths at least as great as 13 m, and such wave forcing is more important than wind forcing in the along-shelf momentum balance in the surf zone (Feddersen et al., 1998; Lentz et al., 1999). For our case, moorings EC5 and EC6 are located at the 10m isobath, but far from the surf zone. Omission of wave radiation stress in our calculations appears warranted by the relatively weak wave regime of the WFS.

9. Summary

Based on multi-year observations of currents, bottom pressures, temperatures, winds, coastal sea levels, and hydrographic data, the depth-averaged momentum balance on the WFS is diagnosed on synoptic and longer time scales. These observational analyses complement previous WFS momentum balance diagnoses performed with numerical models. The following results are presented.

The across-shelf momentum balance on the inner shelf is essentially geostrophic between the Coriolis force due to the along-shelf currents and the

across-shelf bottom pressure gradient, as reported elsewhere (Brown et al., 1985, 1987; Lentz et al., 1999, etc.). The across-shelf wind stress accounts for most of the variance in the ageostrophic momentum residual. During severe weather events, the across-shelf wind stress may even be the dominant term in the across-shelf momentum balance. This supports model results on the importance of the across-shelf wind stress on the inner shelf (Li and Weisberg, 1999a,b; Tilburg, 2003). Taking the across-shelf pressure gradient and the friction (surface and bottom) terms as the forcing functions we account for 95% of the variance in the acceleration (Coriolis plus local) on the inner shelf over the synoptic weather band.

The balances are more complicated on the outer shelf where the Coriolis, the across-shelf bottom pressure gradient, and the horizontal density gradient terms all have the same magnitude. The latter term (representing baroclinicity) plays an increasingly important role as the depth and stratification increase. Outer shelf variability is influenced by deep ocean forcing along with the local winds. Such deep ocean forcing, however, is generally limited to the region of the shelf slope and break by virtue of the Taylor–Proudman theorem. If the shelf is wide enough, as is the case for the WFS, then the inner and outer shelf regions are separated by what we refer to as the mid-shelf, with these inner, mid, and outer shelf regions all being controlled by different dynamical balances.

The along-shelf momentum balance on the inner shelf is primarily between the wind stress and the bottom stress terms, complemented by the pressure gradient and the Coriolis and local acceleration terms. This result agrees with previous studies (Mitchum and Sturges, 1982; Lentz and Winant, 1986; Lee et al., 1989; Lentz et al., 1999). It also supports the Li and Weisberg (1999b) finding that the inner shelf is the region of transition from a near shore balance between surface and bottom stress to a mid-shelf balance between surface stress and Coriolis force (an Ekman balance).

At synoptic weather and longer time scales, the along-shelf wind stress is the dominant driver of the along-shelf currents on the inner shelf. The bottom friction, pressure gradient, and Coriolis terms are consequences of this. An along-shelf pressure gradient is set up by the local wind stress and acts in opposite to it. It thereby accounts for a smaller fraction of the along-shelf velocity variance than the along-shelf wind stress. These features distinguish

the inner WFS from the inner shelf of northern California, where the along-shelf wind stress and pressure gradient tend to be similar in magnitude (Lentz, 1994), the Pacific Northwest Shelf, where the along-shelf pressure gradient is primarily of non-local origin (Hickey, 1984), and the central Southern California Bight where the along-shelf pressure gradient accounts for a much larger fraction of the along-shelf velocity than the local wind stress (Hickey et al., 2003).

It is demonstrated that the depth-averaged, along-shelf currents on the inner shelf may be estimated from the winds and coastal sea level or from the winds and the across-shelf bottom pressure gradient, or from both. The across-shelf sea level gradient on the inner shelf may also be inferred from the wind and coastal sea level data. A simple average of these two approaches provides an improved estimate of the along-shelf currents and the across-shelf sea level gradient.

Inferred from these analyses depending on the bottom stress parameterization are a drag coefficient C_D of $2\text{--}4 \times 10^{-3}$ and a resistance coefficient r of $3\text{--}6 \times 10^{-4} \text{ m s}^{-1}$.

Acknowledgements

Support was by the Office of Naval Research, Grant numbers N00014-98-1-0158 and N00014-02-1-0972. The second of these, which is for the Southeast Atlantic Coastal Ocean Observing System (SEACOOS), is administered by UNC under Task order # 3-12110-10. Observations were also supported by the National Oceanic and Atmospheric Administration, Grant # NA76RG0463. G. Vargo and C. Heil provided the hydrographic data. The USF Ocean Circulation Group assisted in all aspect of the data collection and analysis. R. Cole and C. Merz facilitated the mooring deployments at sea. J. Donovan, W. Hemme, R. Helber, R. He, D. Mayer, P. Smith and V. Subramanian helped with data processing.

References

- Bendat, T.S., Pierson, A.G., 1986. *Random Data: Analysis and Measurement Procedures*. Wiley, New York 566pp.
- Blumberg, A.F., Mellor, G.L., 1987. A description of a three-dimensional coastal ocean circulation model. In: Heaps, N. (Ed.), *Three-dimensional Coastal Ocean Models*, Coastal and Estuarine Sciences, vol. 4. American Geophysical Union, Washington, DC, pp. 208–233.

- Brown, W.S., Irish, J.D., Winant, C.D., 1987. A description of subtidal field observations on the northern California during the coastal ocean dynamics experiment. *Journal of Geophysical Research* 92 (C2), 1605–1635.
- Brown, W.S., Pettigrew, N.R., Irish, J.D., 1985. The Nantucket shoals flux experiment (NSFE79), II. The structure and variability of across-shelf pressure gradients. *Journal of Physical Oceanography* 15, 749–771.
- Chuang, W.-S., Wiseman, W.J., 1983. Coastal sea level response to frontal passages on the Louisiana–Texas Shelf. *Journal of Geophysical Research* 88 (C4), 2615–2620.
- Feddersen, F., Guza, R.T., 2003. Observations of nearshore circulation: alongshore uniformity. *Journal of Geophysical Research* 108 (C1), 3006.
- Feddersen, F., Guza, R.T., Elgar, S., Herbers, T.H.C., 1998. Alongshore momentum balances in the nearshore. *Journal of Geophysical Research* 103 (C8), 15667–15676.
- Feddersen, F., Guza, R.T., Elgar, S., Herbers, T.H.C., 2000. Velocity moments in alongshore bottom stress parameterizations. *Journal of Geophysical Research* 105 (C4), 8673–8686.
- Gilbes, F., Tomas, C., Walsh, J.J., Muller-Karger, F.E., 1996. An episodic chlorophyll plume on the West Florida Shelf. *Continental Shelf Research* 16 (9), 1201–1224.
- Grant, W.D., Williams III, A.J., Glenn, S.M., 1984. Bottom stress estimates and their prediction on the Northern California continental shelf during CODE-1: the importance of wave–current interaction. *Journal of Physical Oceanography* 14, 506–527.
- Harms, S., Winant, C.D., 1994. Synthetic subsurface pressure derived from bottom pressure and tide gauge observations. *Journal of Atmospheric and Oceanic Technology* 11, 1625–1637.
- He, R., Weisberg, R.H., 2002a. West Florida shelf circulation and temperature budget for the 1999 spring transition. *Continental Shelf Research* 22, 719–748.
- He, R., Weisberg, R.H., 2002b. Tides on the West Florida Shelf. *Journal of Physical Oceanography* 32 (12), 3455–3473.
- He, R., Weisberg, R.H., 2003. A Loop Current intrusion case study on the west Florida shelf. *Journal of Physical Oceanography* 33 (2), 465–477.
- He, R., Liu, Y., Weisberg, R.H., 2004. Coastal ocean wind fields gauged against the performance of an ocean circulation model. *Geophysical Research Letters* 31, L14303.
- Hetland, R.D., Hsueh, Y., Leben, R.R., Niiler, P.P., 1999. A loop current induced jet along the edge of the West Florida Shelf. *Geophysical Research Letter* 26, 2239–2242.
- Hickey, B.M., 1984. The fluctuating longshore pressure gradient on the Pacific Northwest shelf: a dynamical analysis. *Journal of Physical Oceanography* 14, 276–293.
- Hickey, B.M., Dobbins, E.L., Allen, S.E., 2003. Local and remote forcing of currents and temperature in the central Southern California Bight. *Journal of Geophysical Research* 108 (C3), 3081.
- Huh, O.K., Wiseman, W.J., Rouse, L.J., 1981. Intrusion of loop current waters onto the West Florida continental shelf. *Journal of Geophysical Research* 86 (C5), 4186–4192.
- Large, W.G., Pond, S., 1981. Open ocean momentum flux measurements in moderate to strong winds. *Journal of Physical Oceanography* 11, 324–336.
- Lee, T.N., Ho, W.J., Kourafalou, V., Wang, J.D., 1984. Circulation on the continental shelf of the Southeastern United States, I. Subtidal response to wind and Gulf Stream forcing during winter. *Journal of Physical Oceanography* 14, 1001–1012.
- Lee, T.N., Williams, E., Wang, R.E.J., Atkinson, L., 1989. Response of South Carolina continental shelf waters to wind and Gulf Stream forcing during winter of 1986. *Journal of Geophysical Research* 94, 10715–10754.
- Lentz, S., 1994. Current dynamics over the Northern California inner shelf. *Journal of Physical Oceanography* 24, 2461–2478.
- Lentz, S., Trowbridge, J.H., 2001. A dynamical description of fall and winter mean profiles over the northern California shelf. *Journal of Physical Oceanography* 31, 914–930.
- Lentz, S., Winant, C.D., 1986. Subinertial currents on the South California shelf. *Journal of Physical Oceanography* 16, 1737–1750.
- Lentz, S., Guza, R.T., Elgar, S., Feddersen, F., Herbers, T.H.C., 1999. Momentum balance on the North Carolina inner shelf. *Journal of Geophysical Research* 104, 18205–18226.
- Li, Z., Weisberg, R.H., 1999a. West Florida Shelf response to upwelling favorable wind forcing: kinematics. *Journal of Geophysical Research* 104, 13507–13527.
- Li, Z., Weisberg, R.H., 1999b. West Florida continental shelf response to upwelling favourable wind forcing, 2, Dynamics. *Journal of Geophysical Research* 104, 23427–23442.
- Mellor, G.L., Mechoso, C.R., Keto, E., 1982. A diagnostic calculation of the general circulation of the Atlantic Ocean. *Deep Sea Research* 29 (10A), 1171–1192.
- Mitchum, G.T., Sturges, W., 1982. Wind-driven currents on the West Florida Shelf. *Journal of Physical Oceanography* 12, 1310–1317.
- Molinari, R.L., Baig, S., Behringer, D.W., Maul, G.A., Legeckis, R., 1977. Winter intrusions of the loop current. *Science* 198, 505–506.
- Morison, J., 1991. Seasonal fluctuations in the West Spitsbergen Current estimated from bottom pressure measurements. *Journal of Geophysical Research* 96 (C10), 18381–18395.
- Paluszkievicz, T., Atkinson, L.P., Posmentier, E.S., McClain, C.R., 1983. Observations of a loop current frontal eddy intrusion onto the west Florida Shelf. *Journal of Geophysical Research* 88 (C14), 9639–9651.
- Pawlowicz, R., Beardsley, B., Lentz, S., 2002. Classical tidal harmonic analysis including error estimates in MA-TLAB using T_TIDE. *Computers & Geosciences* 28, 929–937.
- Thompson, K.R., Pugh, D.T., 1986. The subtidal behaviour of the Celtic Sea—II Currents. *Continental Shelf Research* 5, 321–346.
- Tilburg, C.E., 2003. Across-shelf transport on a continental shelf: do across-shelf winds matter? *Journal of Physical Oceanography* 33, 2675–2688.
- Tilburg, C.E., Garvine, R.W., 2003. Three-dimensional flow in a coastal upwelling zone: convergence and divergence on the New Jersey Shelf. *Journal of Physical Oceanography* 33, 2113–2125.
- Trowbridge, J.H., Lentz, S.J., 1998. Dynamics of the bottom boundary layer on the northern California shelf. *Journal of Physical Oceanography* 28, 2075–2093.
- Wearn Jr., R.B., Larson, N.G., 1982. Measurements of the sensitivities and drift of Digiquartz pressure sensors. *Deep Sea Research* 29, 111–134.

- Weisberg, R.H., He, R., 2003. Local and deep-ocean forcing contributions to anomalous water properties on the West Florida Shelf. *Journal of Geophysical Research* 108 (C6), 3184.
- Weisberg, R.H., Black, B., Li, Z., 2000. An upwelling case study on Florida's west coast. *Journal of Geophysical Research* 105, 11459–11469.
- Weisberg, R.H., Li, Z., Muller-Karger, F.E., 2001. West Florida shelf response to local wind forcing: April 1998. *Journal of Geophysical Research* 106, 31239–31262.
- Winant, C.D., Beardsley, R.C., 1979. A comparison of some shallow wind-driven currents. *Journal of Physical Oceanography* 9, 218–220.